Applied Thermal Engineering 114 (2017) 1213–1221

Contents lists available at ScienceDirect

Applied Thermal Engineering

journal homepage: www.elsevier.com/locate/apthermeng

Research Paper

Estimation of the surface thermal resistances and heat loss by conduction using thermography

Beatriz M. Marino, Natalia Muñoz, Luis P. Thomas *

Geophysical and Environmental Flows Group, CIFICEN (CONICET – UNCPBA - CICPBA), Pinto 399, 7000 Tandil, Argentina

HIGHLIGHTS

- A technique to quantify heat loss by conduction through the building envelope is introduced.
- Heat flux calculation without using tabulated surface thermal resistances.
- IR thermography is employed to obtain surface temperatures of a representative construction.
- U-values and in-situ measurements are combined to estimate surface thermal resistances.
- Contributions of building envelope materials to the total heat loss are estimated.

ARTICLE INFO

Article history:
Received 30 December 2015
Revised 26 October 2016
Accepted 7 December 2016
Available online 9 December 2016

Keywords:
Infrared thermography
Heat loss
Surface thermal resistance
In-situ measurements
Actual use conditions

ABSTRACT

The thermal insulation of a construction is established by the resistances of the materials employed and the thermal surface resistances, which may vary significantly from one building to another because of its location and climatic conditions. The importance of the surface resistances has been underestimated probably due to its complex calculation and variability since they depend on the differences of temperature and humidity, wind, shape of the envelope, surrounding obstacles such as trees, and other buildings. In this work, infrared thermography is employed to obtain the internal and external surface temperatures of the façades of a representative construction as part of a methodology to quantify the heat loss by conduction through the building envelope. *U*-values that encompass the characteristics of the envelope components and the thermal surface resistances are used. It is found that the thermal resistances of the air boundary layers vary during the day and, in most cases, are much greater than the values currently suggested by local regulations, thus significantly reducing the effective thermal conductivity of the envelope with respect to the design value. The findings show how important it is to quantitatively determine the heat flux through the building envelope on site for an already existing construction and corroborate the value estimated in the design stage.

1. Introduction

Approximately a third of the energy produced in Argentina is used for the management of buildings [1]. Of this amount, almost half is employed to satisfy the demand of heating and cooling, while more than 30% of the rest is lost by insufficient or damaged thermal insulation in roofs and walls that, therefore, are prone to present heat leaks in winter and overheating in summer. In parallel, it is estimated that at present, buildings are responsible for more than 40% of global energy use and one third of global greenhouse gas emissions, primarily through the use of fossil fuels during their operational phase, both in developed and developing countries [2]. The importance of this topic is related to the scarcity of resources and global warming.

In this context, the detection and quantification of heat losses through building envelopes become relevant. In Argentina, the IRAM standards on thermal conditioning of buildings are employed to estimate the heat loss by conduction through building constructive systems and thermal properties of the construction materials, under steady-state conditions by means of the *U-value* method commonly used (see §4), and employing tabulated constant values of the surface thermal resistances. These regulations are mandatory for new constructions and for the remodeling of more than 50% of the building's area in several provinces. However, although the estimation of these parameters is useful to guide architects and engineers during the design stage, the values under actual use

* Corresponding author.
E-mail addresses: bmarino@exa.unicen.edu.ar (B.M. Marino), nmvasquez@gmail.com (N. Muñoz), lthomas@exa.unicen.edu.ar (L.P. Thomas).

http://dx.doi.org/10.1016/j.applthermaleng.2016.12.033
1359-4311/

Nomenclature

A	total surface area (m^2)
e	thickness (m)
FF	first floor
GF	ground floor
h_e	external convective coefficient (W/m^2 K)
k	thermal conductivity of the material (W/m K)
K	thermal transmittance (W/m^2 K)
q	heat flux per unit area (W/m^2)
Q	heat flux lost by conduction (W)
r	reflectivity
R	thermal resistance (m^2 K/W)
R_{si}	internal surface thermal resistance (m^2 K/W)
R_{se}	external surface thermal resistance (m^2 K/W)
T	absolute temperature (K)
T_i	internal temperature (°C)
T_e	external temperature (°C)
T_1	internal side temperature (°C)
T_2	external side temperature (°C)
T_r	background temperature (°C)
U	overall thermal transmittance or overall heat transfer coefficient
α	absorptivity
α_l	absorptivity of long-wave thermal radiation
α_s	absorptivity of short-wave thermal radiation
ε	emissivity
λ	wavelength (μm)
τ	transmissivity

conditions may be different according to the type of construction, variety and updating of materials, ageing, local geographic characteristics, etc. In the case of old buildings, the lack of information about them complicates the energetic assessment, thus necessarily implying the estimation of the heat flux between spaces, and between external and internal environments.

To describe the response of the buildings to the temporal changes of the outside temperature, in addition to the thermal transmittance, the thermal capacity and the density of the materials must be considered. These changes produce two important effects: the attenuation of the energy flux with the wall thickness (or decrement factor), and a time lag between the maximum values of the temperature difference and the heat fluxes at both sides of the wall. In this case, the periodic solution of the heat equation may be obtained by means of the admittance procedure [3] described, for example, in ISO 13786 standards [4] and following, and in Ref. [5]. However, in some cases the effect of the thermal inertia of the building envelope depends on the time of the day. Fokaides and Kalogirou [6] determined the *U*-values of typical building constructions in Cyprus at different daytime hours and validated their results with the theoretical values obtained from EN standards, achieving reliable *U*-values under a quasi-steady state condition early in the morning and late at night with an acceptable error of 10–20%.

If the *U*-value method is applied, as the overall thermal transmittance *U* is related to the thermal transmittance *K* and the surface thermal resistances, the determination of the surface resistances is an issue of great importance to the proper estimation of the heat transfer.

On the other hand, the ease and rapid operation of the thermographic cameras to carry out measurements in inaccessible surfaces and in a non-invasive way make thermography a widely applied technique in fields such as building and electrical installation inspections [7–11], industrial environments [12,13] and in difficult access objects [14], but also in medicine and veterinary science [15,16], and in the non-destructive evaluation of damages of cultural heritage artworks [17] and hybrid laminates [18]. Together with traditional techniques of the constructions monitoring, thermography is a valuable tool to detect building envelope defects such as heat losses, missing or damaged insulation in walls and roofs, thermal bridges, infiltrations, air leakage and moisture sources [19,20]. As a complement of thermo-energetic audits, it is particularly important to locate problematic areas that may otherwise go undetected, and to measure surface temperatures of walls, roofs and floors.

However, despite the significant progress in the performance of the infrared cameras and in the analysis of the images, today's thermographic studies present limitations as, for example, distortion of the thermographic lens and lack of geo-referenced temperature data. To obtain quantitative reliable measurements, the emissivity of the surface, the distance between the thermal camera and the assessed object, the absorption of infrared radiation by air and the background temperature must be known to prevent adverse effects on the precision of the images. For a long time, little progress was achieved in the use of thermography to carry out quantitative evaluations of the heat flux through a building envelope because of the especial care that is required to obtain surface temperature distributions [21–24]. Most recently, infrared thermography was applied to assess the thermal transmittance *U* of walls [6,25–29].

In this work, infrared thermography is employed to determine the temperature of the façade and side walls of a building whose standards of construction are representative of an Argentinean geographic region. This helps to better estimate the heat flux exchanged with the exterior and the heat losses by conduction through the building envelope, but also makes it possible to calculate the external and internal surface thermal resistances and consider their influence on the total thermal resistance. This study is limited to the steady-state case because the heat capacity of the materials does not significantly affect the heat flux through the envelope of the assessed building [3], and in order to compare the results with the ones obtained by the traditional *U*-value method. In the next section the theoretical basis of thermography are revisited; then, the methodology applied and instruments employed are described. Following this, results are introduced and discussed, and finally conclusions are given.

2. Theoretical background

Radiation enables the energy transfer between a surface and its surrounding by means of the absorption, reflection and emission of electromagnetic waves. Unlike heat conduction and convection that need a medium to transport energy, radiation is transmitted through the empty space or the air with null or little attenuation. The radiation emitted by a real object depends on the kind of surface and its temperature *T*. Of our interest is the radiation resulting of indirect (or reflected) radiation provided by the sun or by artificial lights, and the near and far infrared radiation emitted by the objects at ambient temperature ($T \sim 300$ K), sometimes named "short-wave" and "long-wave" thermal radiation, respectively. The wavelength λ of the short-wave radiation is between 0.2 μm and 3.0 μm, is characteristic of the high temperature sources ($T > 3000$ K) and includes the near-ultraviolet

(0.20 μm < λ < 0.38 μm), visible (0.38 μm < λ < 0.78 μm) and near-infrared (0.78 μm < λ < 3.0 μm) spectra. Long-wave thermal radiation covers the medium and far infrared radiation with 3.0 μm < λ < 50 μm. Both kinds of radiation are absorbed partly by materials, but the latter is also partly emitted.

The absorptivity α indicates the part of the incident radiation that is absorbed by the surface, while the rest is reflected (specified by the reflectivity r) and/or transmitted (specified by the transmissivity τ) if the surface is partly transparent. In a steady-state, the energy conservation principle implies that $\alpha + r + \tau = 1$. The absorptivity, reflectivity and transmissivity of a given material depend on λ. The absorbed radiation is also dissipated through the air in contact with the surface by convection, or it is released to the exterior as infrared radiation. The absorptivity α_s of short-wave thermal radiation is characteristic of each material and ranges between 0.1 and 0.95, while the absorptivity α_l of long-wave thermal radiation has the same value of emissivity ε that is defined as the ratio of the energy radiated from that surface to that radiated from a blackbody at the same temperature.

A frequent way to classify the surfaces is by determining whether they are reflective if α_s, τ < 20–25% or they behave similar to black bodies if α_s, ε > 80–85% [30]. Alternately, materials can be classified according to its reflectivity. Thus, reflective surfaces have high reflectivity (r > 0.80–0.85) while the black bodies have low reflectivity (r < 0.20–0.25). Both classifications relate to each other when they are applied to opaque bodies ($\tau \sim 0$) for which a high value of r corresponds to a low value of α, and viceversa. For buildings, however, it is convenient to compare the visible and near-infrared radiations for the incident radiation, and the visible and far-infrared radiation for the reflected radiation. Consequently, it is possible to differentiate the hot (α_s > 80–85%, ε < 20–25%) and cold (α_s < 20–25%, ε > 80–85%) selective surfaces, in addition to the reflective and those that behave as black bodies [30].

Most materials employed in constructions are opaque ($\tau \approx 0$, $\alpha + r \approx 100\%$) to infrared radiation, and mostly have high emissivity ($\varepsilon \approx 0.90$–0.95%) as is the case of white-painted or red brick walls of the building assessed in this study [30,31]. Standard glazed surfaces are also opaque to the far-infrared radiation (λ > 3 μm) and have high emissivity with similar values, in addition to their well-known transparency to the visible radiation and specular reflection. This is especially important to perform measurements with a thermographic camera.

3. Methodology

The assessed building is the Central Library (Fig. 1) situated in the Campus of *Universidad Nacional del Centro de la Provincia de Buenos Aires*, in the semi-urban area of Tandil City (37°19′S - 59°08′O), in the center-east of Buenos Aires Province (Argentina). The local climate is template and humid with mild summers and intermediate temperature amplitudes (about 15° C) throughout the year. Meteorological typical values in Tandil are presented in Table 1 according to the bio-environmental classification of Argentina [32]. According to local regulations, it is recommended that the design of buildings have very good insulation throughout the envelope, twice the insulation on roofs as that in the walls, the use of the thermal inertia to reduce the thermal amplitude effect, the control of infiltrations, application of displacement ventilation in summer, and a glazing - opaque surface relationship not greater than 15%. In addition, the solar resource is not significant in winter because of the high cloudiness registered in the zone.

The equipment used in this work was a thermographic camera FLUKE TiR32 that measures the temperatures in a range from −20 °C to 150 °C with a thermal resolution of 0.04 °C at 30 °C. The detectors form a focal plane array of 320 × 240 pixels. It captures the thermal radiation emitted or reflected by the surface of objects in the range 7.5 < λ < 14 μm, and proportionally transforms the energy received by each pixel in intensity. In this way the corresponding temperature distribution is determined.

The emissivity values of the different materials and the compensation for reflected background temperature T_r are set in accordance with the usual procedures as those recommended by Melgosa Revillas [33] and the ASTM standards [34–36]. Basically, a piece of crumpled aluminium foil is placed onto the measurement region captured by the infrared image. The reading of the aluminium foil temperature was made at a distance of 1 m setting the infrared camera emissivity level to 1. This is the background temperature T_r. Then, black vinyl electrical tape which has emissivity values of 0.95 ± 0.05 is applied onto the wall. Setting the infrared camera emissivity level to 0.95 and the T_r value previously obtained, the temperature on the tape is measured. Finally, the black tape is withdrawn and the temperature of the wall surface is measured, varying the emissivity value until the wall temperature reaches the black tape temperature.

The distance (∼3 m) between the tested surface and the camera, dimensions of the building and thickness of walls and glazed surfaces were measured with a FLUKE 414D laser distance meter with a precision of 1 mm. At this distance, the attenuation of the infrared radiation and the reduction of image sharpness due to air are negligible [31]. To avoid the effect of the reflectivity on the measurements, particularly in the cases of glazed surfaces, different angles were tested ranging from 0° to 30° from surface normal. Some measurements of the wall temperature were checked with a digital Smartmeter thermometer and a thermo-resistance PT-100 class 1/3, stuck to the surface, which measures with a precision of ±0.1 °C. To assess errors in temperatures obtained using the infrared camera, a number of controlled measurements were performed on the different envelope components over a range of temperatures and environmental conditions. From these tests, the overall error due to uncertainty of the emissivity of the envelope components, the reflected background temperature and the camera response is smaller than 0.7 °C.

Fig. 1. View from the west of the assessed building.

Table 1
Typical values of the meteorological parameters in Tandil (Buenos Aires, Argentina).

Symbol	Description	Summer (January-February-March)	Winter (June-July-August)
TMXA	Absolute maximum temperature (°C)	37.4	25.4
TMAX	Mean maximum temperature (°C)	26.4	14.1
TMED	Mean temperature (°C)	19.5	8.5
THUM	Apparent temperature (°C)	16.2	6.2
TMIN	Mean minimum temperature (°C)	13.3	2.9
TMA	Absolute minimum temperature (°C)	3.6	−11.6
TROC	Dew temperature (°C)	13.7	4.5
TVAP	Partial water vapour pressure (hPa)	16.2	8.8
TDMN	Minimum design temperature (°C)	9.1	−6.6
TDMX	Maximum design temperature (°C)	34.9	16.2
HR	Relative humidity (%)	71.2	80.0
VM	Mean wind speed (km/h)	14.8	13.4
PREC	Average precipitation (mm)	377	180
NUB	Cloudiness	3.6	4.6
CLA	Days with clear sky/month	10.0	6.0
CUB	Days with overcast sky/month	6.0	12.0
PRE	Rainy days/month	8.0	7.0
GRA	Days with hail/month	0	0
NEV	Days with snowfall/month	0	0.1
NIE	Days with fog/month	4.0	10.0
HEL	Days with frost/month	0	8.0
TOR	Days with storms/month	6.0	2.0
HEF	Effective heliophany	7.7	4.4
HELRE	Relative heliophany	58.0	42.0
PRAT	Air pressure (hPa)	990.5	995.2
GD18	Heating degree days (18 °C, annual)		1839
GD20	Heating degree days (20 °C, annual)		2409
GD22	Heating degree days (22 °C, annual)		3046

Two series of measurements were performed in winter between 9 and 16 June (2014), and between 8 and 16 July (2014) at 7:00–8:00, 13:00–14:00, 17:00–18:00. Data obtained in windy and/or rainy weather were ruled out. The four façades of the building envelope are composed by 6 types of repeated architectural components and combine bricks walls and large glass windows. The locations of these components in the ground floor are indicated in Fig. 2, photos of some sectors are shown in Fig. 3, while Fig. 4 displays the thermogram and photograph of the component 2 taken early in the morning on 14 July. All glazed surfaces are made of double pane 0.020, 0.024 and 0.028 m thick glass with thermal transmittances $k/e = 3.20$, 3.20 and 2.8 W/m^2 K, respectively, where e is the thickness and k is the specific thermal conductivity of the material. The masonry consists of a face brick wall 0.12 m thick, a panel of expanded polystyrene 0.035 m thick, a waterproofing coating, a porotherm brick wall 0.12 m thick, and two layers of plaster on the inner side, fulfilling the regulations for constructions in this Argentinean geographic zone. All the walls of the envelope are 0.30 m thick with $k/e = 0.72$ W/m^2 K as calculated following the procedure indicated in IRAM 11601 [37] without considering the surface resistances. When variations of the outdoor temperature exist, in addition to the thermal transmittances, heat capacity and density of the materials must be considered, since the heat flux through the envelope may be reduced and delayed. However, according to Muñoz et al. [3], the effects of the outdoor temperature changes are not important for this specific building and, therefore, the assumption of a steady-state heat flux through the envelope is an acceptable approximation. The calculation reported in this work involves the vertical plane surfaces of the envelope. The thermal behavior of the aluminium frames of the glazed panels, the cylindrical sectors located on the building corners, the metallic locks of the boilers, the roof and the floor have special characteristics and the estimation of their contributions to the total heat loss by conduction through the envelope will be reported elsewhere.

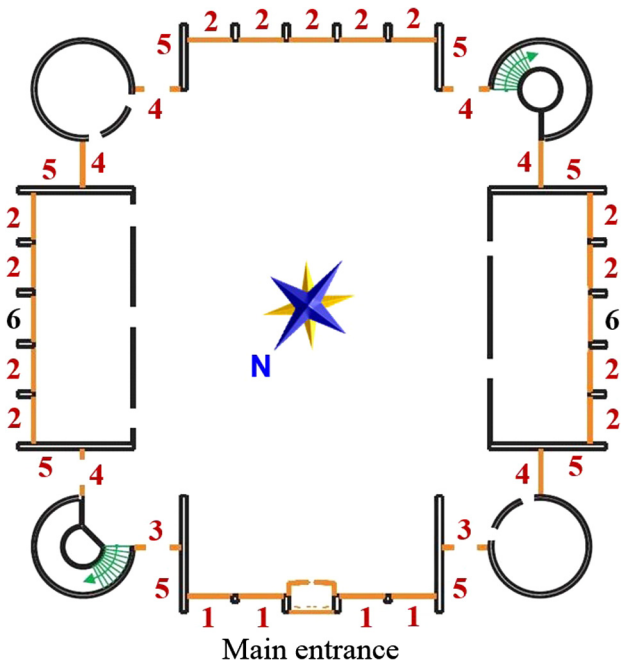

Fig. 2. Sketch of the ground floor (similar to the first floor) of the building indicating the location of the building envelope components. 1: Glass panels in the front face, 2: Walls and windows, 3, 4: Glass doors and panels out of the perimeter, 5: Walls, 6: Boilers locks.

The internal temperatures T_i of the ground and first floors of the Central Library building were determined averaging the data provided by two sensors HOBO U12 placed in each floor in specific points of the huge central atrium. These sensors measure every 10 min with a precision of ±0.35 °C and a resolution of 0.03 °C at 25 °C. The external temperature T_e was measured by a weather station Decagon Em50 located 200 m from the building.

4. Estimation of the heat flux through the building envelope

The heat flux by conduction per unit area q (or heat flux density in W/m^2) through the building envelope is

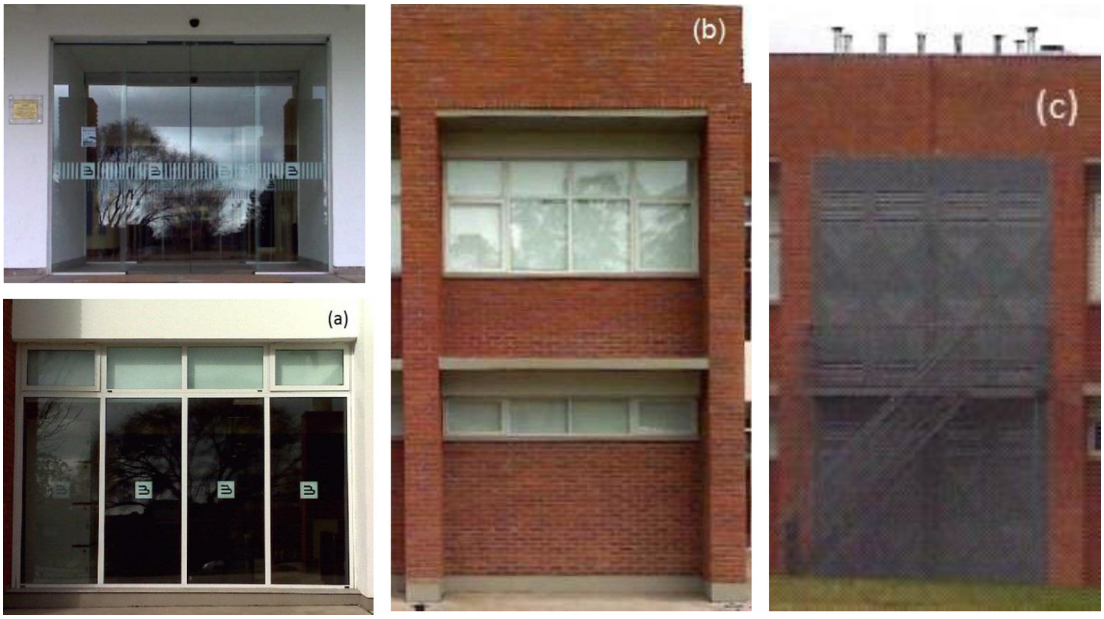

Fig. 3. Some external sectors of the assessed building: (a) Main entrance (above) and Component 1 (below) situated on the ground floor, (b) Component 2 (ground and first floors), and (c) Component 6 (ground and first floors).

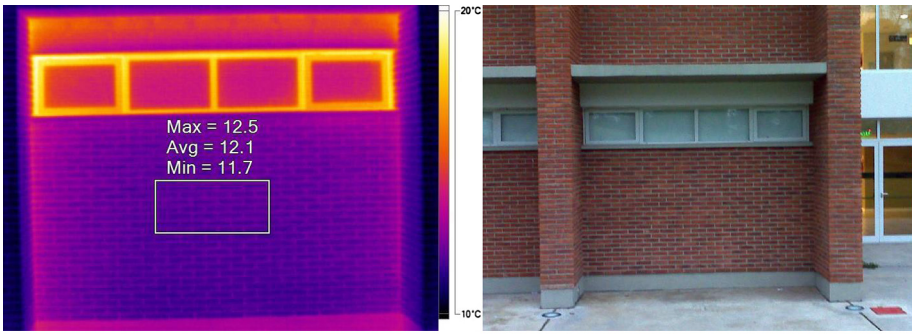

Fig. 4. Thermogram and photograph of the northeast-facing component 2 (ground floor) of the building envelope, exterior temperature 9 °C.

$$q = U(T_e - T_i), \tag{1}$$

where U is measured in $Wm^{-2}\,K^{-1}$. In the cases of walls and openings to the outside, the U value is obtained by means of the overall thermal resistance R:

$$R = \frac{1}{U} = R_{si} + \frac{e}{k} + R_{se} \tag{2}$$

where R_{si} and R_{se} are the surface thermal resistances of the internal and external air boundary layers, respectively, of the building envelope. For a given material of thickness e, the value of k is tabulated. The heat transfer by natural convection from a vertical plane depends, in fact, on the regime in the air boundary layer (laminar or turbulent), the plane height that is considered as a characteristic distance, and the Rayleigh number. The equation describing the heat transfer is further complicated by the wind action in mixed convection (natural and forced convections acting simultaneously). Because of the complexity of the estimation of R_{si} and R_{se}, constant values are adopted by the standards as shown in Table 2 for R_{se}, in order to choose the most appropriate building envelope component materials. It is also common to relate the external convective coefficient h_e to the wind [32]. However, the surface resistances for an already existing building can be calculated by the methodology described next.

Table 2
Values of R_{se} to different standards.

Standards	$R_{se}{}^{-1} = h_e$ (W/m^2 K)
IRAM 11601 (Argentina)	25
CIBSE (United Kingdom)	17
ASHRAE (United States of America)	22.7 (summer) – 34.0 (winter)
ENER (Mexico)	13

The temperatures of the internal and external sides (T_1 and T_2, respectively) are functions of the inside and outside temperatures (T_i and T_e, respectively) (Fig. 5). The steady-state heat flux is the same in all layers and its value is given by Eq. (1) that, using Eq. (2), becomes:

$$q\left(R_{si} + \frac{e}{k} + R_{se},\right) = (T_i - T_e) \tag{3}$$

Then,

$$qR_{si} = T_i - T_1, \tag{4a}$$

$$q\frac{e}{k} = T_1 - T_2, \tag{4b}$$

$$qR_{se} = T_2 - T_e, \tag{4c}$$

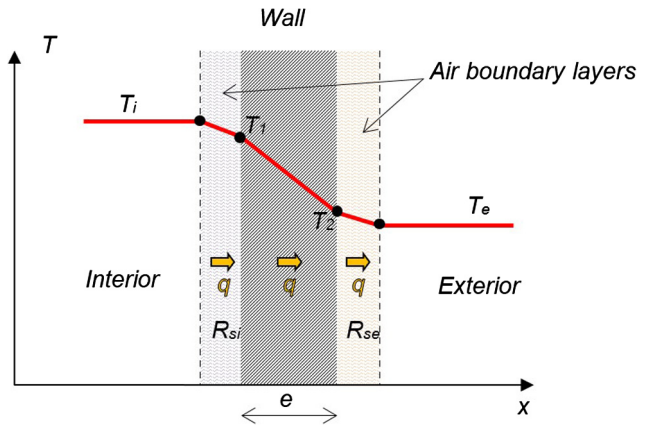

Fig. 5. Temperature profile across a wall considering the air boundary layers of the building envelope.

and the relative resistances are:

$$\frac{R_{si}}{R} = \frac{T_i - T_1}{T_i - T_e}, \tag{5a}$$

$$\frac{e/k}{R} = \frac{T_1 - T_2}{T_i - T_e}, \tag{5b}$$

$$\frac{R_{se}}{R} = \frac{T_2 - T_e}{T_i - T_e}. \tag{5c}$$

The heat flux lost by conduction through the total surface area A is $Q = qA$. Eqs. (4) and (5) show the importance of measuring the surface temperatures under actual use conditions, and not only in the laboratory under controlled conditions (by using, for example, the heat flow meter method). Here the heat flux q is estimated by means of Eq. (4b) measuring T_1 and T_2 with the thermographic camera and considering the thickness e and thermal conductivity k of material in every case. Then, the surface resistances are calculated by Eqs. (4a) and (4c).

5. Results and discussion

Fig. 6 shows the evolution of temperatures T_i, T_1 and T_2 in the glass panels (component 1 in Fig. 2) and T_e while Fig. 7 illustrates the evolution of the relative differences of temperature $(T_i - T_1)/(T_i - T_e)$ and $(T_2 - T_e)/(T_i - T_e)$ associated with R_{si} and R_{se} (Eq. (5)), respectively. These measurements correspond to the façade facing the northwest. It is interesting to note that these differences have similar values to those of $(T_1 - T_2)/(T_i - T_e)$ (represented by asterisks in Fig. 7) associated with the material resistance. Therefore, the thermal resistances of both air boundary layers are as important as the thermal resistance of the material, thus implying that the values of R_{si} and R_{se} are different from those of the design and change with the component location and hour of the day. At noon, $T_1 \approx T_i$ probably because the solar radiation heats the air close to the glazed surfaces facing the northwest. In this case, R_{si} is negligible and the total resistance becomes $R = R_{se} + e/k$.

Table 3 shows that the thermal resistances R_{si} of the glazed surfaces are of the same order of, or smaller than, the value currently suggested by IRAM 11601 (that is, 0.13 m^2 K/W), while those of the walls are more than twice this value. On the contrary, thermal surface resistances R_{se} are much greater than the suggested for walls and glazed surfaces (that is, 0.04 m^2 K/W), thus significantly reducing the effective thermal conductivity of the envelope with respect to the design value.

The values of R_{si}/R, $e/(kR)$ and R_{se}/R, calculated using Eq. (5) which are based on the temperature measurements, corresponding to the different constructive components of the building envelope and hours of the day, are averaged and presented in Table 4. The spatial and temporal variations of R_{si} and R_{se} confirm the influence of the complex dynamics of the air boundary layers, as mentioned above, due to the presence of other nearby walls, the different solar radiation and wind effect acting on each building envelope component. These factors change throughout the day; the greater fluctuations taking place at midday. Without underestimating the significance of these changes, it is important to obtain the mean representative values of the heat flux per unit area, q.

Using Eq. (4b) with the values of T_1 and T_2 measured early in the morning and in the evening, the heat flux lost through each component is related to the temperature difference $(T_i - T_e)$ as shown in Fig. 8a for the glazed surfaces in the building front façade (components 1) and in Fig. 8b for the side walls (components 2). The best fit lines determined by using the method of least squares have a standard deviation of 0.27 in both cases and the adjusted R-square is equal to 0.51 and 0.42 for data fitted in Fig. 8a and b, respectively. Note also that the relationship between the heat flux q and the temperature difference $(T_i - T_e)$ has a different slope (that is, U – Eq. (1)) according to the material and location (since

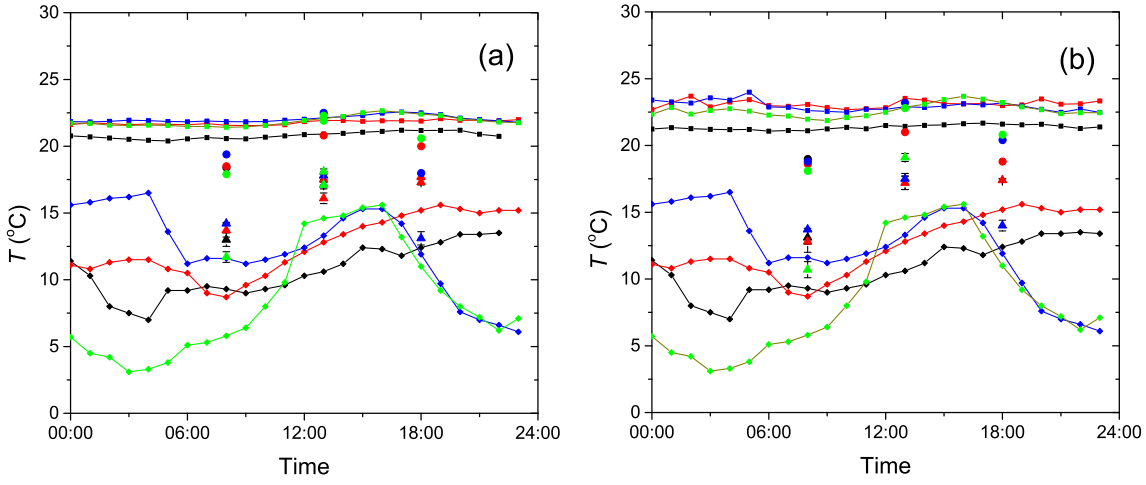

Fig. 6. Evolution of indoor temperatures (T_i, squares), temperatures on internal (T_1, circles) and external (T_2, triangles) faces of glazing surfaces, and outdoor temperatures (T_e, diamonds) for the ground (a) and first (b) floors, registered on 16 June (black), and 14 (red), 15 (blue) and 16 (green) July 2014. The error bars and symbols are of about similar size. (For interpretation of the references to colour in this figure legend, the reader is referred to the web version of this article.)

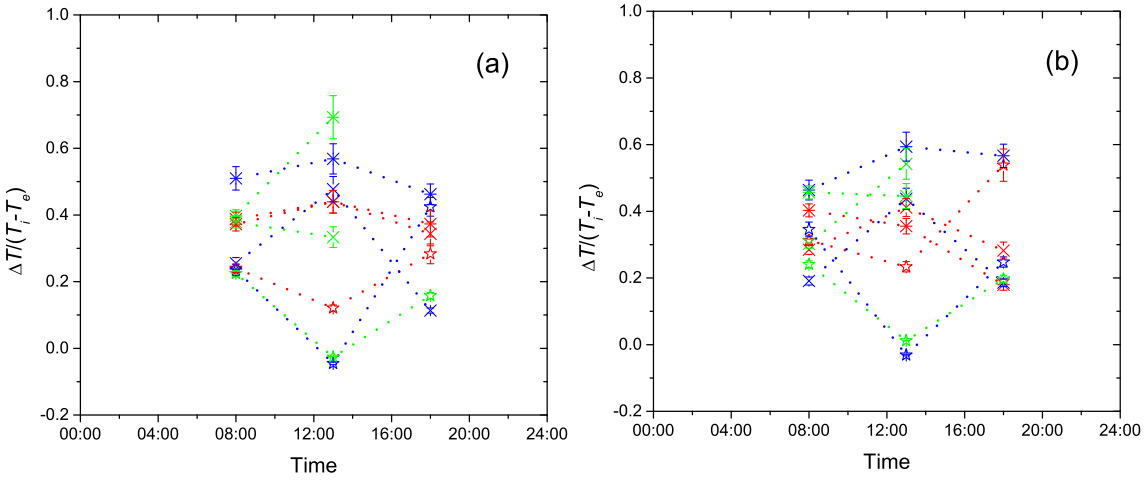

Fig. 7. Temperature relative difference between the interior and the internal face of glass windows (open stars), $(T_i - T_1)/(T_i - T_e)$, between internal and external faces of the glass window (asterisk), $(T_1 - T_2)/(T_i - T_e)$, and between the external face and the exterior (cross), $(T_2 - T_e)/(T_i - T_e)$, corresponding to 14 (red), 15 (blue) and 16 (green) July 2014. (a) Ground floor; (b) First floor. (For interpretation of the references to colour in this figure legend, the reader is referred to the web version of this article.)

Table 3
Mean values of the thermal surface resistances of the building envelope components indicated in Fig. 2, for the ground and first floors.

		Component 1 (Glazed surfaces)			Component 2 (Windows)			Component 3 (Glazed doors and panels)		
		8:00h	13:00h	18:00h	8:00h	13:00h	18:00h	8:00h	13:00h	18:00h
GF	R_{si}	0.103	0.038	0.09	0.069	0.046	0.113	0.089	–	0.074
	R_{se}	0.106	0.130	0.071	0.106	0.113	0.063	0.157	0.196	0.199
FF	R_{si}	0.093	0.073	0.103	0.102	0.100	0.123	–	–	–
	R_{se}	0.081	0.145	0.073	0.083	0.099	0.023	–	–	–
		Component 4 (Glazed doors and panels)			Component 5 (Walls)			Component 2 (Side walls)		
		8:00h	13:00h	18:00h	8:00h	13:00h	18:00h	8:00h	13:00h	18:00h
GF	R_{si}	0.070	0.044	0.101	0.240	0.157	0.303	0.215	0.354	0.326
	R_{se}	0.104	0.107	0.032	0.574	0.813	0.629	0.264	0.520	0.078
FF	R_{si}	–	–	–	0.404	0.294	0.355	0.301	0.463	0.430
	R_{se}	–	–	–	0.465	0.676	0.636	0.223	0.381	0.046

Table 4
Mean values of R_{si}/R, $e/(kR)$ and R_{se}/R calculated with Eq. (5) and overall thermal transmittance of the building envelope components. The values of U are the slopes of lines that best fit experimental points as in Fig. 8.

		Component 1 (Glazed surfaces)			Component 2 (Windows)			Component 3 (Glazed doors and panels)		
		8:00h	13:00h	18:00h	8:00h	13:00h	18:00h	8:00h	13:00h	18:00h
GF	R_{si}/R	0.233	0.121	0.289	0.221	0.146	0.362	0.250	0.093	0.207
	$e/(kR)$	0.439	0.441	0.490	0.444	0.439	0.439	0.308	0.359	0.413
	R_{se}/R	0.340	0.417	0.228	0.338	0.363	0.394	0.439	0.547	0.556
	U (W/m^2 K)	1.5			1.5			0.8		
FF	R_{si}/R	0.299	0.234	0.328	0.326	0.319	0.394			
	$e/(kR)$	0.456	0.406	0.357	0.467	0.456	0.456			
	R_{se}/R	0.259	0.464	0.234	0.265	0.318	0.072			
	U (W/m^2 K)	1.5			1.5					
		Component 4 (Glazed doors and panels)			Component 5 (Walls)			Component 2 (Side walls)		
		8:00h	13:00h	18:00h	8:00h	13:00h	18:00h	8:00h	13:00h	18:00h
GF	R_{si}/R	0.225	0.140	0.323	0.173	0.113	0.218	0.155	0.255	0.235
	$e/(kR)$	0.523	0.727	0.670	0.416	0.303	0.485	0.656	0.433	0.665
	R_{se}/R	0.334	0.341	0.104	0.574	0.813	0.629	0.264	0.520	0.078
	U (W/m^2 K)	1.9			0.3			0.45		
FF	R_{si}/R	–	–	–	0.291	0.212	0.256	0.216	0.333	0.309
	$e/(kR)$	–	–	–	0.375	0.299	0.304	0.633	0.440	0.640
	R_{se}/R	–	–	–	0.465	0.676	0.636	0.223	0.381	0.046
	U (W/m^2 K)				0.3			0.45		

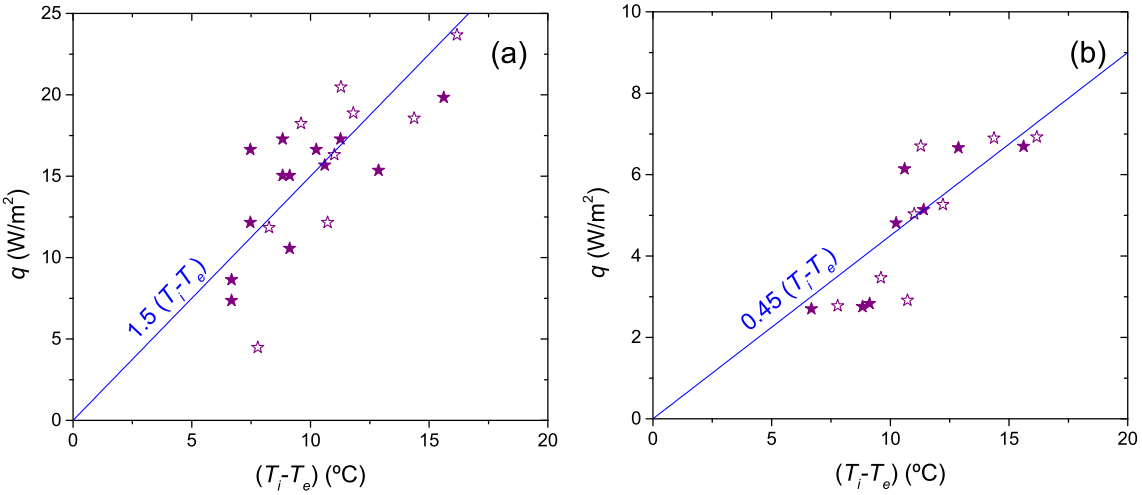

Fig. 8. Heat flux per unit area lost through the Components 1 (a) and 2 (b) of the building in the ground (solid symbols) and first (open symbols) floors as function of the temperature difference between indoors and outdoors.

the surface resistances are different). Linear dependencies such as those found in these figures are observed for the rest of the envelope components, except for some values corresponding to walls obtained at noon when the sky is clear. In these cases $T_2 > T_i$ because of the solar heating of the walls, thus verifying the existence of an inwards heat flux. For this reason, the contribution of this particular heat flux is not considered in the mean values presented in Tables 4 and 5. However, the main value of the total heat flux Q is not affected because most of the measurements were performed in cloudy days; in addition, the walls contribution plays a secondary role as it is inferred from the results shown in Table 4. In effect, 53% of the surface of the envelope concerned is glazed, which contributes with 83% to the total heat flux thanks to its greater thermal conductivity with respect to that of the walls, as observed in Table 5 where the individual contribution of each constructive component to the total heat flux Q (in W and %) lost during the days in which measurements were performed are shown together with the corresponding e, k/e, U, A. The time variation of the total heat flux Q is illustrated in Fig. 9. This information is very useful especially because the assessed building is a part of the university campus where there are no gauges of gas and electricity consumption in each building.

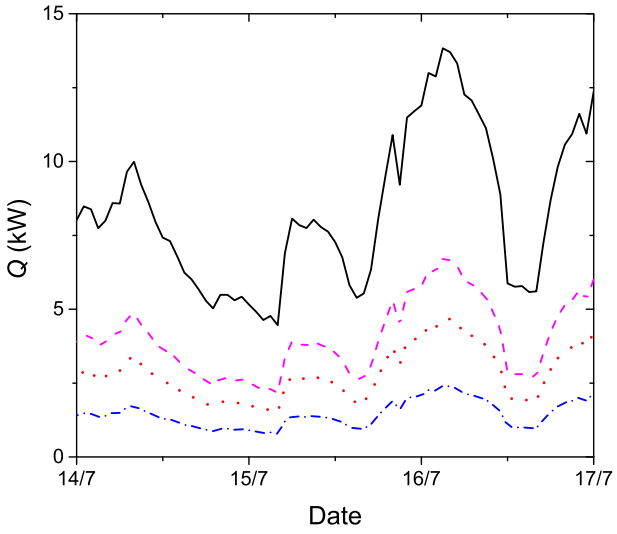

Fig. 9. Evolution of the total heat flux lost by conduction (solid line) and contributions to Q from the glazing openings of the northwest façade (dashed line), glass openings located away from the building line (dotted line) and walls (dashed-dotted line).

6. Conclusions

Infrared thermography is employed to obtain the internal and external surface temperatures of the façades of a building considered as a study case and, together the inside and outside air temperatures measured independently, to estimate the heat flux through the building envelope. The methodology takes advantage of air's transparency to the infrared radiation emitted by the surfaces over short distances, thus enabling measurements of the surface temperature *in-situ* and the collection of information that is difficult to acquire by other means. For example, it is possible to quantify the change of the resistances of the air boundary layers during the day in different parts of the building, or detect the accumulation of heat in the walls due to solar radiation.

Representative values of the heat flux by conduction were found for the vertical plane surfaces of the ground and first floors of the assessed building. From the measurements, it is observed that the thermal resistance of materials is similar to the surface thermal resistance for both glasses and walls. Thus, the overall

Table 5
Characteristic parameters of the building envelope components and total heat flux Q lost through each of them during the measuring days.

N°	Components:	e (m)	k/e (W/m² K)	U (W/m² K)	A (m²)	Q (W)	Q (%)
1	Glass panels, front face	0.024	3.2	1.5	91.09	136.64	19.5
2	Windows	0.024	3.2	1.5	136.52	204.78	29.2
3	Glass doors and panels out of the perimeter, front face	0.028	2.8	0.8	37.21	29.77	4.2
4	Glass doors and panels out of the perimeter, lateral faces	0.02	3.2	1.9	111.43	211.72	30.2
5	Walls, lateral faces	0.3	0.72	0.3	230.92	69.28	9.9
2	Walls under the windows, lateral faces	0.3	0.72	0.45	109.24	49.16	7.0
	Total:				**716.42**	**701.34**	**100.0**

thermal resistance U^{-1} of the envelope concerned is about twice the thermal resistance of materials.

In order to facilitate the calculation of the surface thermal resistances, the radiation contribution was neglected. Consistently, the R_{se} values measured at noon were dismissed to estimate the mean value of q in Table 5 and Fig. 8. If radiation is considered, T_e should be replaced by an equivalent temperature known as *sun-air temperature*, defined as the outside air temperature for which, in the absence of radiation, the external environment delivers the same heat flux to the wall surface [9]. Nevertheless, the total inward heat flux through the building envelope consists of the conduction (Fig. 9) and radiation contributions.

Another factor that needs to be further considered is the dynamic response of the building envelope. The heat transfer through the walls is reduced and delayed by the corresponding decrement factor and time lag, while these parameters are negligible for double pane windows and doors. However, such effects are not significant in the building assessed here. Indeed, employing the dynamic coefficients reported in [3], the values of the surface resistances are not significantly affected, but the heat lost through the glasses reaches 88% of total instead of 83% reported in the previous section, emphasizing that the glazing surfaces are the largest contributor to the heat loss by conduction. In addition, the U values were estimated from temperatures measured in the morning and in the evening when temporal changes of the outdoor temperature are small to be taken into account, thus minimising errors related to the use of the time-independent model of the heat transfer by conduction. Nevertheless, a more comprehensive study may be needed to assess other type of constructions.

The results are valid for this building under the conditions of the measurement during the days indicated, but they show the importance of the quantitative estimations of the heat flux in buildings after the construction. Future studies will include the analysis of the accumulation of heat in the walls and the effects of some factors (meteorology, location of the sunshades and recesses of the building envelope, direction and intensity of the prevailing winds, etc.) on the estimations of the thermal surface resistances.

Acknowledgements

The research was financed by the ANPCyT by means of PICT 2202/12.

References

[1] Industrial Technology National Institute (INTI) Ahorro y certificación energética: la envolvente de los edificios. *Saber cómo*. N° 27, pp. 4, Argentina, 2005. Available from: <http://www.inti.gob.ar/sabercomo/sc27/inti5.php>.
[2] UNEP- SBCI United Nations Environment Programme, Sustainable Buildings & Climate Initiative, Buildings and Climate Change. Summary for Decision-Makers, 2009, Available from: <http://www.unep.org/sbci/pdfs/SBCI-BCCSummary.pdf>.
[3] N. Muñoz, L.P. Thomas, B.M. Marino, Comportamiento térmico dinámico de muros típicos empleando el método de la admitancia, Energías Renovables y Medio Ambiente 36 (2015) 31–39.
[4] ISO 13786, Thermal Performance of Building Components - Dynamic Thermal Characteristics - Calculation Methods, European Committee of Standardization, Brussels, Belgium, 2007.
[5] B. Anderson, S. Doran, K. Mina, G. Pettit, Thermal properties of building structures, in: K. Butcher (Ed.), CIBSE Guide Book A: Environmental Design, Chartered Institution of Building Service Engineers, London, UK, 2015.
[6] P.A. Fokaides, S.A. Kalogirou, Application of infrared thermography for the determination of the overall heat transfer coefficient (U-value) in building envelopes, Appl. Energy 88 (12) (2011) 4358–4365.
[7] N.P. Avdelidis, A. Moropoulou, Applications of infrared thermography for the investigation of historic structures, J. Cult. Herit. 5 (2004) 119–127.
[8] A. Rahman Al-Kassir, J. Fernandez, F.V. Tinaut, F. Castro, Thermographic study of energetic installations, Appl. Therm. Eng. 25 (2005) 183–190.
[9] F. Sandrolini, E. Franzoni, An operative protocol for reliable measurements of moisture in porous materials of ancient buildings, Build. Environ. 41 (2006) 1372–1380.
[10] T.M. Lindquist, L. Bertling, Hazard rate estimation of high-voltage contacts using infrared thermography, in: Annual Reliability and Maintainability Symposium, Las Vegas, NV, USA (28–31 January 2008), 233–239, Available from: <http://doi.ieeecomputersociety.org/10.1109/RAMS.2008.4925800>.
[11] C. Balaras, A. Argirou, Infrared thermography for building diagnostics, Energy Build. 34 (2002) 171–183.
[12] A. Chrysochoos, B. Berthel, F. Latourte, Local energy analysis of high-cycle fatigue using digital image correlation and infrared thermography, J. Strain Anal. Eng. 43 (6) (2008) 411–421.
[13] P. McMullan, Assessing structural components of new masonry construction utilizing infrared thermography, in: Thermosense XII: An International Conference on Thermal Sensing and Imaging Diagnostic Applications, Orlando, Florida, United States (1 March 1990) Proc SPIE 1313, 78, Available from <http://dx.doi.org/10.1117/12.21913>.
[14] M.R. Clark, D.M. McCann, M.C. Forde, Application of infrared thermography to the non-destructive testing of concrete and masonry bridges, NDT&E Int. 36 (2003) 265–275.
[15] J.R. Keyserling, P.D. Ahlgren, E. Yu, N. Belliveau, M. Yassa, Functional infrared imaging of the breast–historical perspectives, current applications and future considerations, IEEE Eng. Med. Biol. Mag. 19 (3) (2000) 33–41.
[16] D.J. McCafferty, The value of infrared thermography for research on mammals: previous applications and future directions, Mammal Rev. 37 (3) (2007) 207–223.
[17] S. Sfarra, C. Ibarra-Castanedo, D. Paoletti, X. Maldague, Infrared vision inspection of cultural heritage objects from the city of L'Aquila, Italy and its surroundings, Mater. Eval. 71 (5) (2013) 561–570.
[18] S. Sfarra, C. Ibarra-Castanedo, C. Santulli, F. Sarasini, D. Ambrosini, D. Paoletti, X. Maldague, Eco-friendly laminates: from the indentation to non-destructive evaluation by optical and infrared monitoring techniques, Strain 49 (2) (2013) 175–189, http://dx.doi.org/10.1111/str.12026.
[19] S. Martín, I. Cañas, I. González, Thermographic survey of two rural buildings in Spain, Energy Build. 34 (2004) 515–523.
[20] E. Rosina, J. Spodek, Using infrared thermography to detect moisture in historic masonry: a case study in Indiana, APT Bull. 34 (2009) 11–16.
[21] R.J. Goldstein, Application of aerial infrared thermography to the measurement of building heat loss, ASHRAE Trans. 84 (1978) 207–226.
[22] R.T. Mack, Energy loss profiles: foundation for future profit in thermal imager sales and service, in: 5th Infrared Information Exchange, New Orleans, USA, 1985, pp. 15–24.
[23] E. Grinzato, P.G. Bison, G. Cesini, R. Ricci, Quality control of cold store assembling by IR thermography and numerical simulation. I.I.F. Commission B2, C2, Dl, D2, D3. Dresden, Germany, 743–748, 1990.
[24] E. Grinzato, V. Vavilov, T. Kauppinen, Quantitative infrared thermography in buildings, Energy Build. 29 (1998) 1–9.
[25] G. Dall'O, L. Sarto, A. Panza, Infrared screening of residential buildings for energy audit purposes: results of a field test, Energies 6 (2013) 3859–3878.
[26] R. Albatici, A.M. Tonelli, Infrared thermovision technique for the assessment of thermal transmittance value of opaque building elements on site, Energy Build. 42 (2010) 2177–2183.
[27] R. Albatici, A.M. Tonelli, M. Chiogna, A comprehensive experimental approach for the validation of quantitative infrared thermography in the evaluation of building thermal transmittance, Appl. Energy 141 (2015) 218–228.
[28] I. Nardi, S. Sfarra, D. Ambrosini, Quantitative thermography for the estimation of the U-value: state of the art and a case study, J. Phys: Conf. Ser. 547 (1) (2014) 012016.
[29] I. Nardi, D. Paoletti, D. Ambrosini, T. de Rubeis, S. Sfarra, U-value assessment by infrared thermography: a comparison of different calculation methods in a Guarded Hot Box, Energy Build. 122 (2016) 211–221.
[30] M. DeKay, G.Z. Brown, Sun, Wind, and Light: Architectural Design Strategies, third ed., John Wiley & Sons Lt, Chichester, 2013.
[31] M.Y.L. Chew, Assessing building façades using infra-red thermography, Struct. Survey 16 (2) (1998) 81–86.
[32] IRAM 11603, Acondicionamiento térmico de edificios: Clasificación bioambiental de la República Argentina, Instituto Argentino de Normalización y Certificación, Buenos Aires, 2011. Available from: <www.iram.org.ar>.
[33] S. Melgosa Revillas, Guía de la termografía infrarroja, Aplicaciones en ahorro y eficiencia energética, Fundación de la Energía de la Comunidad de Madrid, 2011, Available from: <http://www.fenercom.com/pages/publicaciones/publicacion.php?id=168>.
[34] ASTM C1046-95, Standard Practice for In-Situ Measurement of Heat Flux and Temperature on Building Envelope Components, ASTM International, West Conshohocken, PA, 2013, Available from: <www.astm.org>.
[35] ASTM C1153-97, Standard Practice for Location of Wet Insulation in Roofing Systems Using Infrared Imaging, ASTM International, West Conshohocken, PA, 2003, Available from: <www.astm.org>.
[36] ASTM C1060-11a, Standard Practice for Thermographic Inspection of Insulation Installations in Envelope Cavities of Frame Buildings, ASTM International, West Conshohocken, PA, 2011, Available from: <www.astm.org>.
[37] IRAM 11601, Aislamiento térmico de edificios Métodos de cálculo Propiedades térmicas de los componentes y elementos de construcción en régimen estacionario, Instituto Argentino de Normalización y Certificación, Buenos Aires, Argentina, 2002.